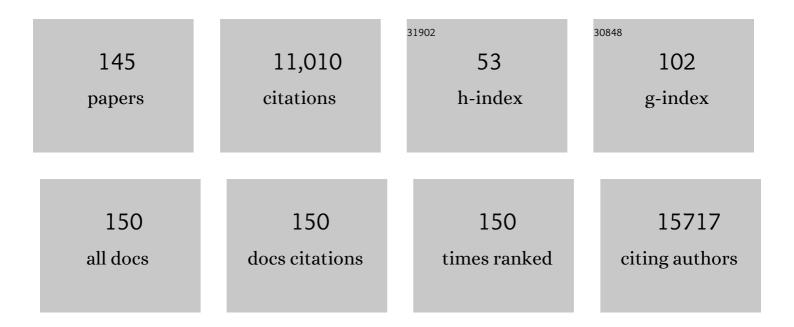
List of Publications by Year in descending order

Source: https://exaly.com/author-pdf/2549550/publications.pdf Version: 2024-02-01



IIAN-RIN XII

#	Article	IF	CITATIONS
1	High-responsivity graphene/silicon-heterostructure waveguide photodetectors. Nature Photonics, 2013, 7, 888-891.	15.6	731
2	Hybrid Halide Perovskite Solar Cell Precursors: Colloidal Chemistry and Coordination Engineering behind Device Processing for High Efficiency. Journal of the American Chemical Society, 2015, 137, 4460-4468.	6.6	586
3	Graphene and related two-dimensional materials: Structure-property relationships for electronics and optoelectronics. Applied Physics Reviews, 2017, 4, .	5.5	476
4	Near-Infrared Photodetector Based on MoS ₂ /Black Phosphorus Heterojunction. ACS Photonics, 2016, 3, 692-699.	3.2	446
5	Flexible Piezoelectric-Induced Pressure Sensors for Static Measurements Based on Nanowires/Graphene Heterostructures. ACS Nano, 2017, 11, 4507-4513.	7.3	435
6	Room temperature high-detectivity mid-infrared photodetectors based on black arsenic phosphorus. Science Advances, 2017, 3, e1700589.	4.7	419
7	Two-dimensional quasi-freestanding molecular crystals for high-performance organic field-effect transistors. Nature Communications, 2014, 5, 5162.	5.8	315
8	Electronic Properties of MoS ₂ –WS ₂ Heterostructures Synthesized with Two-Step Lateral Epitaxial Strategy. ACS Nano, 2015, 9, 9868-9876.	7.3	283
9	Analyzing the Carrier Mobility in Transitionâ€Metal Dichalcogenide MoS ₂ Fieldâ€Effect Transistors. Advanced Functional Materials, 2017, 27, 1604093.	7.8	265
10	Highly Sensitive Glucose Biosensors Based on Organic Electrochemical Transistors Using Platinum Gate Electrodes Modified with Enzyme and Nanomaterials. Advanced Functional Materials, 2011, 21, 2264-2272.	7.8	243
11	Highâ€Performance Grapheneâ€Based Hole Conductorâ€Free Perovskite Solar Cells: Schottky Junction Enhanced Hole Extraction and Electron Blocking. Small, 2015, 11, 2269-2274.	5.2	233
12	A self-powered high-performance graphene/silicon ultraviolet photodetector with ultra-shallow junction: breaking the limit of silicon?. Npj 2D Materials and Applications, 2017, 1, .	3.9	211
13	Synergistic Effects of Plasmonics and Electron Trapping in Graphene Short-Wave Infrared Photodetectors with Ultrahigh Responsivity. ACS Nano, 2017, 11, 430-437.	7.3	192
14	1T′ Transition Metal Telluride Atomic Layers for Plasmon-Free SERS at Femtomolar Levels. Journal of the American Chemical Society, 2018, 140, 8696-8704.	6.6	192
15	Lateral Builtâ€In Potential of Monolayer MoS ₂ –WS ₂ Inâ€Plane Heterostructures by a Shortcut Growth Strategy. Advanced Materials, 2015, 27, 6431-6437.	11.1	191
16	Recent Advances of Solution-Processed Metal Oxide Thin-Film Transistors. ACS Applied Materials & Interfaces, 2018, 10, 25878-25901.	4.0	183
17	Highly Confined and Tunable Hyperbolic Phonon Polaritons in Van Der Waals Semiconducting Transition Metal Oxides. Advanced Materials, 2018, 30, e1705318.	11.1	178
18	2D materials–based homogeneous transistor-memory architecture for neuromorphic hardware. Science, 2021, 373, 1353-1358.	6.0	177

#	Article	IF	CITATIONS
19	Electron Mobility Exceeding 10 cm ² V ^{â^'1} s ^{â^'1} and Bandâ€Like Charge Transport in Solutionâ€Processed nâ€Channel Organic Thinâ€Film Transistors. Advanced Materials, 2016, 28, 5276-5283.	11.1	173
20	Ultrahigh mobility and efficient charge injection in monolayer organic thin-film transistors on boron nitride. Science Advances, 2017, 3, e1701186.	4.7	146
21	High Responsivity, Broadband, and Fast Graphene/Silicon Photodetector in Photoconductor Mode. Advanced Optical Materials, 2015, 3, 1207-1214.	3.6	141
22	Facile and Environmentally Friendly Solution-Processed Aluminum Oxide Dielectric for Low-Temperature, High-Performance Oxide Thin-Film Transistors. ACS Applied Materials & Interfaces, 2015, 7, 5803-5810.	4.0	139
23	Epitaxial Ultrathin Organic Crystals on Graphene for Highâ€Efficiency Phototransistors. Advanced Materials, 2016, 28, 5200-5205.	11.1	134
24	The role of solution-processed high-κ gate dielectrics in electrical performance of oxide thin-film transistors. Journal of Materials Chemistry C, 2014, 2, 5389.	2.7	133
25	Centimeter-Scale CVD Growth of Highly Crystalline Single-Layer MoS ₂ Film with Spatial Homogeneity and the Visualization of Grain Boundaries. ACS Applied Materials & Interfaces, 2017, 9, 12073-12081.	4.0	120
26	Graphene controlled Brewster angle device for ultra broadband terahertz modulation. Nature Communications, 2018, 9, 4909.	5.8	117
27	Fusedâ€Ring Electron Acceptor ITICâ€Th: A Novel Stabilizer for Halide Perovskite Precursor Solution. Advanced Energy Materials, 2018, 8, 1703399.	10.2	112
28	Effects of Alkyl Chain Length on Crystal Growth and Oxidation Process of Two-Dimensional Tin Halide Perovskites. ACS Energy Letters, 2020, 5, 1422-1429.	8.8	112
29	Highly Sensitive and Broadband Organic Photodetectors with Fast Speed Gain and Large Linear Dynamic Range at Low Forward Bias. Small, 2017, 13, 1603260.	5.2	102
30	A Simple Method for Synthesis of Highâ€Quality Millimeterâ€Scale 1T′ Transitionâ€Metal Telluride and Nearâ€Field Nanooptical Properties. Advanced Materials, 2017, 29, 1700704.	11.1	101
31	Ag-Doped Halide Perovskite Nanocrystals for Tunable Band Structure and Efficient Charge Transport. ACS Energy Letters, 2019, 4, 534-541.	8.8	96
32	Nonstoichiometric acid–base reaction as reliable synthetic route to highly stable CH3NH3PbI3 perovskite film. Nature Communications, 2016, 7, 13503.	5.8	94
33	Precise, Self-Limited Epitaxy of Ultrathin Organic Semiconductors and Heterojunctions Tailored by van der Waals Interactions. Nano Letters, 2016, 16, 3754-3759.	4.5	92
34	High-Performance Broadband Floating-Base Bipolar Phototransistor Based on WSe ₂ /BP/MoS ₂ Heterostructure. ACS Photonics, 2017, 4, 823-829.	3.2	89
35	Flexible dielectric papers based on biodegradable cellulose nanofibers and carbon nanotubes for dielectric energy storage. Journal of Materials Chemistry C, 2016, 4, 6037-6044.	2.7	88
36	Monolayer Fieldâ€Effect Transistors of Nonplanar Organic Semiconductors with Brickwork Arrangement. Advanced Materials, 2015, 27, 3418-3423.	11.1	85

#	Article	IF	CITATIONS
37	General Nondestructive Passivation by 4â€Fluoroaniline for Perovskite Solar Cells with Improved Performance and Stability. Small, 2018, 14, e1803350.	5.2	82
38	Hybrid graphene tunneling photoconductor with interface engineering towards fast photoresponse and high responsivity. Npj 2D Materials and Applications, 2017, 1, .	3.9	77
39	Largeâ€Grain Formamidinium PbI _{3–} <i>_x</i> Br <i>_x</i> for Highâ€Performance Perovskite Solar Cells via Intermediate Halide Exchange. Advanced Energy Materials, 2017, 7, 1601882.	10.2	76
40	In-Plane Optical Absorption and Free Carrier Absorption in Graphene-on-Silicon Waveguides. IEEE Journal of Selected Topics in Quantum Electronics, 2014, 20, 43-48.	1.9	75
41	Crystallinity Preservation and Ion Migration Suppression through Dual Ion Exchange Strategy for Stable Mixed Perovskite Solar Cells. Advanced Energy Materials, 2017, 7, 1700118.	10.2	74
42	Epitaxial Stitching and Stacking Growth of Atomically Thin Transitionâ€Metal Dichalcogenides (TMDCs) Heterojunctions. Advanced Functional Materials, 2017, 27, 1603884.	7.8	73
43	Ultrathin efficient perovskite solar cells employing a periodic structure of a composite hole conductor for elevated plasmonic light harvesting and hole collection. Nanoscale, 2016, 8, 6290-6299.	2.8	69
44	Fully Biodegradable Water Droplet Energy Harvester Based on Leaves of Living Plants. ACS Applied Materials & Interfaces, 2020, 12, 56060-56067.	4.0	69
45	Performance and Stability Improvement of P3HT:PCBM-Based Solar Cells by Thermally Evaporated Chromium Oxide (CrO _{<i>x</i>}) Interfacial Layer. ACS Applied Materials & Interfaces, 2010, 2, 2699-2702.	4.0	68
46	Interlayer Interaction Enhancement in Ruddlesden–Popper Perovskite Solar Cells toward High Efficiency and Phase Stability. ACS Energy Letters, 2019, 4, 1025-1033.	8.8	64
47	A Meaningful Analogue of Pentacene: Charge Transport, Polymorphs, and Electronic Structures of Dihydrodiazapentacene. Chemistry of Materials, 2009, 21, 1400-1405.	3.2	63
48	Fibrous Epoxy Substrate with High Thermal Conductivity and Low Dielectric Property for Flexible Electronics. Advanced Electronic Materials, 2016, 2, 1500485.	2.6	63
49	Perovskite Bifunctional Device with Improved Electroluminescent and Photovoltaic Performance through Interfacial Energyâ€Band Engineering. Advanced Materials, 2019, 31, e1902543.	11.1	62
50	Aqueous Solution-Deposited Gallium Oxide Dielectric for Low-Temperature, Low-Operating-Voltage Indium Oxide Thin-Film Transistors: A Facile Route to Green Oxide Electronics. ACS Applied Materials & Interfaces, 2015, 7, 14720-14725.	4.0	60
51	Strong optical response and light emission from a monolayer molecular crystal. Nature Communications, 2019, 10, 5589.	5.8	59
52	Enhancing lightâ€matter interaction in <scp>2D</scp> materials by optical micro/nano architectures for highâ€performance optoelectronic devices. InformaÄnÃ-MateriA¡ly, 2021, 3, 36-60.	8.5	59
53	Observation of a giant two-dimensional band-piezoelectric effect on biaxial-strained graphene. NPG Asia Materials, 2015, 7, e154-e154.	3.8	58
54	Guanidinium doping enabled low-temperature fabrication of high-efficiency all-inorganic CsPbl ₂ Br perovskite solar cells. Journal of Materials Chemistry A, 2019, 7, 27640-27647.	5.2	56

#	Article	IF	CITATIONS
55	Integration of inverse nanocone array based bismuth vanadate photoanodes and bandgap-tunable perovskite solar cells for efficient self-powered solar water splitting. Journal of Materials Chemistry A, 2017, 5, 19091-19097.	5.2	55
56	Abnormal Synergetic Effect of Organic and Halide Ions on the Stability and Optoelectronic Properties of a Mixed Perovskite via In Situ Characterizations. Advanced Materials, 2018, 30, e1801562.	11.1	55
57	Pushing the Efficiency of High Openâ€Circuit Voltage Binary Organic Solar Cells by Vertical Morphology Tuning. Advanced Science, 2022, 9, e2200578.	5.6	51
58	Growth of Large-Scale, Large-Size, Few-Layered α-MoO ₃ on SiO ₂ and Its Photoresponse Mechanism. ACS Applied Materials & Interfaces, 2017, 9, 5543-5549.	4.0	50
59	Single crystal n-channel field effect transistors from solution-processed silylethynylated tetraazapentacene. Journal of Materials Chemistry, 2011, 21, 15201.	6.7	48
60	Carbon Dot-Based Composite Films for Simultaneously Harvesting Raindrop Energy and Boosting Solar Energy Conversion Efficiency in Hybrid Cells. ACS Nano, 2020, 14, 10359-10369.	7.3	47
61	Synthesis and Characterization of Metallic Janus MoSH Monolayer. ACS Nano, 2021, 15, 20319-20331.	7.3	47
62	Graphene photodetector integrated on silicon nitride waveguide. Journal of Applied Physics, 2015, 117, .	1.1	46
63	Controlled Electrochemical Deposition of Largeâ€Area MoS ₂ on Graphene for Highâ€Responsivity Photodetectors. Advanced Functional Materials, 2017, 27, 1603998.	7.8	45
64	Low-temperature facile solution-processed gate dielectric for combustion derived oxide thin film transistors. RSC Advances, 2014, 4, 54729-54739.	1.7	44
65	An Interlayer with Strong Pb-Cl Bond Delivers Ultraviolet-Filter-Free, Efficient, and Photostable Perovskite Solar Cells. IScience, 2019, 21, 217-227.	1.9	43
66	Hybrid 2Dâ€Material Photonics with Bound States in the Continuum. Advanced Optical Materials, 2019, 7, 1901306.	3.6	43
67	The influence of gate dielectrics on a high-mobility n-type conjugated polymer in organic thin-film transistors. Applied Physics Letters, 2012, 100, 033301.	1.5	41
68	Graphene Based Terahertz Light Modulator in Total Internal Reflection Geometry. Advanced Optical Materials, 2017, 5, 1600697.	3.6	41
69	Ultra‣ow Work Function Transparent Electrodes Achieved by Naturally Occurring Biomaterials for Organic Optoelectronic Devices. Advanced Materials Interfaces, 2014, 1, 1400215.	1.9	40
70	Nanoantenna‧andwiched Graphene with Giant Spectral Tuning in the Visibleâ€ŧoâ€Nearâ€Infrared Region. Advanced Optical Materials, 2014, 2, 162-170.	3.6	39
71	Thicknessâ€Dependent Optical Properties and Inâ€Plane Anisotropic Raman Response of the 2D βâ€In 2 S 3. Advanced Optical Materials, 2019, 7, 1901085.	3.6	39
72	Interlayer Crossâ€Linked 2D Perovskite Solar Cell with Uniform Phase Distribution and Increased Exciton Coupling. Solar Rrl, 2020, 4, 1900578.	3.1	39

#	Article	IF	CITATIONS
73	Understanding Charge Transport in All-Inorganic Halide Perovskite Nanocrystal Thin-Film Field Effect Transistors. ACS Energy Letters, 2020, 5, 2614-2623.	8.8	39
74	High-Quality Monolithic Graphene Films via Laterally Stitched Growth and Structural Repair of Isolated Flakes for Transparent Electronics. Chemistry of Materials, 2017, 29, 7808-7815.	3.2	38
75	Graphene/In ₂ S ₃ van der Waals Heterostructure for Ultrasensitive Photodetection. ACS Photonics, 2018, 5, 4912-4919.	3.2	36
76	van der Waals Transition-Metal Oxide for Vis–MIR Broadband Photodetection via Intercalation Strategy. ACS Applied Materials & Interfaces, 2019, 11, 15741-15747.	4.0	36
77	In Situ Ultrafast and Patterned Growth of Transition Metal Dichalcogenides from Inkjetâ€Printed Aqueous Precursors. Advanced Materials, 2021, 33, e2100260.	11.1	36
78	High-speed infrared two-dimensional platinum diselenide photodetectors. Applied Physics Letters, 2020, 116, .	1.5	33
79	Efficient Slantwise Aligned Dion–Jacobson Phase Perovskite Solar Cells Based on Transâ€1,4â€Cyclohexanediamine. Small, 2020, 16, e2003098.	5.2	33
80	Facile passivation of solution-processed InZnO thin-film transistors by octadecylphosphonic acid self-assembled monolayers at room temperature. Applied Physics Letters, 2014, 104, .	1.5	32
81	Bound-States-in-Continuum Hybrid Integration of 2D Platinum Diselenide on Silicon Nitride for High-Speed Photodetectors. ACS Photonics, 2020, 7, 2643-2649.	3.2	32
82	Realization of vertical and lateral van der Waals heterojunctions using two-dimensional layered organic semiconductors. Nano Research, 2017, 10, 1336-1344.	5.8	30
83	Spectroscopic Study of Electron and Hole Polarons in a High-Mobility Donor–Acceptor Conjugated Copolymer. Journal of Physical Chemistry C, 2013, 117, 6835-6841.	1.5	29
84	Controllable modulation of the electronic properties of graphene and silicene by interface engineering and pressure. Journal of Materials Chemistry C, 2013, 1, 4869.	2.7	28
85	Ternary Bulk Heterojunction Photovoltaic Cells Composed of Small Molecule Donor Additive as Cascade Material. Journal of Physical Chemistry C, 2014, 118, 20094-20099.	1.5	28
86	Uncovering the Electronâ€Phonon Interplay and Dynamical Energyâ€Dissipation Mechanisms of Hot Carriers in Hybrid Lead Halide Perovskites. Advanced Energy Materials, 2021, 11, 2003071.	10.2	28
87	Efficient Electronic Transport in Partially Disordered Co ₃ O ₄ Nanosheets for Electrocatalytic Oxygen Evolution Reaction. ACS Applied Energy Materials, 2020, 3, 3071-3081.	2.5	27
88	Deterministic and Etchingâ€Free Transfer of Largeâ€6cale 2D Layered Materials for Constructing Interlayer Coupled van der Waals Heterostructures. Advanced Materials Technologies, 2018, 3, 1700282.	3.0	26
89	An Acoustic Metaâ€ S kin Insulator. Advanced Materials, 2020, 32, e2002251.	11.1	26
90	Quantitative Analysis of Scattering Mechanisms in Highly Crystalline CVD MoS ₂ through a Self-Limited Growth Strategy by Interface Engineering. Small, 2016, 12, 438-445.	5.2	25

#	Article	IF	CITATIONS
91	Control over Light Soaking Effect in Allâ€Inorganic Perovskite Solar Cells. Advanced Functional Materials, 2021, 31, 2101287.	7.8	25
92	Broadside Nanoantennas Made of Single Silver Nanorods. ACS Nano, 2018, 12, 1720-1731.	7.3	24
93	Enhanced Performance of Polymeric Bulk Heterojunction Solar Cells via Molecular Doping with TFSA. ACS Applied Materials & Interfaces, 2015, 7, 13415-13421.	4.0	23
94	Nearâ€Infrared Photoresponse of Oneâ€Sided Abrupt MAPbI ₃ /TiO ₂ Heterojunction through a Tunneling Process. Advanced Functional Materials, 2016, 26, 8545-8554.	7.8	23
95	ZnO electron transporting layer engineering realized over 20% efficiency and over 1.28 V openâ€circuit voltage in allâ€inorganic perovskite solar cells. EcoMat, 2022, 4, .	6.8	23
96	Enhanced Electrochemical Stability by Alkyldiammonium in Dion–Jacobson Perovskite toward Ultrastable Lightâ€Emitting Diodes. Advanced Optical Materials, 2021, 9, 2100243.	3.6	21
97	Vacuum electron emission with low turn-on electric field from hydrogenated amorphous carbon thin films. Applied Physics Letters, 2001, 79, 141-143.	1.5	20
98	Ternary blend bulk heterojunction photovoltaic cells with an ambipolar small molecule as the cascade material. RSC Advances, 2014, 4, 1087-1092.	1.7	20
99	Induced crystallization of rubrene with diazapentacene as the template. Journal of Materials Chemistry, 2012, 22, 4396.	6.7	19
100	Facet-Dependent Property of Sequentially Deposited Perovskite Thin Films: Chemical Origin and Self-Annihilation. ACS Applied Materials & amp; Interfaces, 2016, 8, 32366-32375.	4.0	19
101	Direct Observation of Charge Injection of Graphene in the Graphene/WSe ₂ Heterostructure by Optical-Pump Terahertz-Probe Spectroscopy. ACS Applied Materials & Interfaces, 2019, 11, 47501-47506.	4.0	19
102	A centrifugal microfluidic pressure regulator scheme for continuous concentration control in droplet-based microreactors. Lab on A Chip, 2019, 19, 3870-3879.	3.1	19
103	Cascade Typeâ€II 2D/3D Perovskite Heterojunctions for Enhanced Stability and Photovoltaic Efficiency. Solar Rrl, 2020, 4, 2000282.	3.1	18
104	Derivitization of pristine graphene for bulk heterojunction polymeric photovoltaic devices. Journal of Materials Chemistry, 2012, 22, 16723.	6.7	16
105	Variable electronic properties of lateral phosphorene–graphene heterostructures. Physical Chemistry Chemical Physics, 2015, 17, 31685-31692.	1.3	16
106	Size and crystallinity control of dispersed VO ₂ particles for modulation of metal–insulator transition temperature and hysteresis. CrystEngComm, 2019, 21, 5749-5756.	1.3	16
107	Electrical switching behavior from ultrathin potential barrier of self-assembly molecules tuned by interfacial charge trapping. Applied Physics Letters, 2010, 96, .	1.5	15
108	Tertiary Amines Differentiated from Primary and Secondary Amines by Active Esterâ€Functionalized Hexabenzoperylene in Field Effect Transistors. Chemistry - an Asian Journal, 2019, 14, 1676-1680.	1.7	15

#	Article	IF	CITATIONS
109	Ultraâ€Narrowband Photodetector with High Responsivity Enabled by Integrating Monolayer Jâ€Aggregate Organic Crystal with Graphene. Advanced Optical Materials, 2021, 9, 2100158.	3.6	15
110	Size Modulation and Heterovalent Doping Facilitated Hybrid Organic and Perovskite Quantum Dot Bulk Heterojunction Solar Cells. ACS Applied Energy Materials, 2020, 3, 11359-11367.	2.5	14
111	The compatibility of methylammonium and formamidinium in mixed cation perovskite: the optoelectronic and stability properties. Nanotechnology, 2021, 32, 075406.	1.3	14
112	Generation and Detection of Strain-Localized Excitons in WS ₂ Monolayer by Plasmonic Metal Nanocrystals. ACS Nano, 2022, 16, 10647-10656.	7.3	14
113	Low-voltage flexible pentacene thin film transistors with a solution-processed dielectric and modified copper source–drain electrodes. Journal of Materials Chemistry C, 2013, 1, 2585.	2.7	12
114	Controlled Synthesis of MoxW1–xTe2 Atomic Layers with Emergent Quantum States. ACS Nano, 2021, 15, 11526-11534.	7.3	12
115	Bifunctional Effects of Trichloro(octyl)silane Modification on the Performance and Stability of a Perovskite Solar Cell via Microscopic Characterization Techniques. ACS Applied Energy Materials, 2020, 3, 3302-3309.	2.5	11
116	Unusual electronic and magnetic properties of lateral phosphorene–WSe2 heterostructures. Journal of Materials Chemistry C, 2016, 4, 6657-6665.	2.7	10
117	Improving the Quality of the Si/Cu ₂ 0 Interface by Methylâ€Group Passivation and Its Application in Photovoltaic Devices. Advanced Materials Interfaces, 2017, 4, 1600833.	1.9	9
118	Defect Etching of Phaseâ€Transitionâ€Assisted CVDâ€Grown 2Hâ€MoTe ₂ . Small, 2021, 17, e2102	14 6. 2	9
119	Configuration-dependent electronic and magnetic properties of graphene monolayers and nanoribbons functionalized with aryl groups. Journal of Chemical Physics, 2014, 140, 044712.	1.2	8
120	Enhanced Photoresponse in Interfacial Gated Graphene Phototransistor With Ultrathin Al ₂ O ₃ Dielectric. IEEE Electron Device Letters, 2018, 39, 987-990.	2.2	8
121	Observation of Strong <i>J</i> -Aggregate Light Emission in Monolayer Molecular Crystal on Hexagonal Boron Nitride. Journal of Physical Chemistry A, 2020, 124, 7340-7345.	1.1	8
122	Growth dynamics and photoresponse of the Wadsley phase V ₆ O ₁₃ crystals. Journal of Materials Chemistry C, 2020, 8, 6470-6477.	2.7	8
123	Influence of Annealing on Raman Spectrum of Graphene in Different Gaseous Environments. Spectroscopy Letters, 2014, 47, 465-470.	0.5	7
124	A novel solid-to-solid electrocatalysis of graphene oxide reduction on copper electrode. RSC Advances, 2015, 5, 87987-87992.	1.7	7
125	Stable field emission with low threshold field from amorphous carbon films due to layer-by-layer hydrogen plasma annealing. Journal of Applied Physics, 2002, 91, 5434-5437.	1.1	6
126	Rapid growth of high quality perovskite crystal by solvent mixing. CrystEngComm, 2016, 18, 1184-1189.	1.3	6

#	Article	IF	CITATIONS
127	Experimental Observation of Ultrahigh Mobility Anisotropy of Organic Semiconductors in the Two-Dimensional Limit. ACS Applied Electronic Materials, 2020, 2, 2888-2894.	2.0	6
128	Towards Scalable Fabrications and Applications of 2D Layered Material-based Vertical and Lateral Heterostructures. Chemical Research in Chinese Universities, 2020, 36, 525-550.	1.3	6
129	Suppressed Phase Segregation in Highâ€Humidityâ€Processed Dion–Jacobson Perovskite Solar Cells Toward High Efficiency and Stability. Solar Rrl, 2021, 5, 2100555.	3.1	6
130	Investigation on the Fano-Type Asymmetry in Atomic Semiconductor Coupled to the Plasmonic Lattice. ACS Photonics, 2021, 8, 3583-3590.	3.2	6
131	Induced Crystallization of Rubrene in Thinâ€Film Transistors (Adv. Mater. 30/2010). Advanced Materials, 2010, 22, .	11.1	4
132	Thermal and illumination effects on a PbI ₂ nanoplate and its transformation to CH ₃ NH ₃ PbI ₃ perovskite. CrystEngComm, 2019, 21, 736-740.	1.3	4
133	40 GHz waveguide-integrated two-dimensional palladium diselenide photodetectors. Applied Physics Letters, 2022, 120, .	1.5	4
134	Synthesis of Multishell Carbon Nanotube Composites via Template Method. Chinese Journal of Chemical Physics, 2011, 24, 206-210.	0.6	2
135	Study of the electron standing wave states in scanning tunneling spectroscopy of Si(111) surface. Surface and Interface Analysis, 2013, 45, 962-967.	0.8	2
136	Perovskite Solar Cells: Largeâ€Grain Formamidinium Pbl _{3–} <i>_x</i> Br <i>_x</i> for Highâ€Performance Perovskite Solar Cells via Intermediate Halide Exchange (Adv. Energy Mater. 12/2017). Advanced Energy Materials, 2017, 7, .	10.2	2
137	Self-assembled dipoles of <i>o</i> -carborane on gate oxide tuning charge carriers in organic field effect transistors. Journal of Materials Chemistry C, 2022, 10, 2690-2695.	2.7	2
138	Polarization dependent loss of graphene-on-silicon waveguides. , 2013, , .		1
139	Phonon Polaritons: Highly Confined and Tunable Hyperbolic Phonon Polaritons in Van Der Waals Semiconducting Transition Metal Oxides (Adv. Mater. 13/2018). Advanced Materials, 2018, 30, 1870091.	11.1	1
140	VERY LOW THRESHOLD ELECTRON FIELD EMISSION FROM AMORPHOUS CARBON FILMS WITH HYDROGEN DILUTION. International Journal of Modern Physics B, 2002, 16, 988-992.	1.0	0
141	Stability Improvement of Polymer Based Solar Cells by Thermally Evaporated Cr2O3 Interfacial Layer. Materials Research Society Symposia Proceedings, 2011, 1312, 1.	0.1	0
142	P-N Junction Formation in Electron-beam Irradiated Graphene Step. Materials Research Society Symposia Proceedings, 2012, 1407, 224.	0.1	0
143	Flexible vertical field-effect transistor based on graphene/silicon heterostructure with ion-gel gate. , 2017, , .		0
144	Hybrid Integration of Black Phosphorus-WSe <inf>2</inf> Heterojunction Photodetector on Silicon Waveguide. , 2018, , .		0

#	Article	IF	CITATIONS
145	Lead Halide Perovskites: Uncovering the Electronâ€Phonon Interplay and Dynamical Energyâ€Dissipation Mechanisms of Hot Carriers in Hybrid Lead Halide Perovskites (Adv. Energy Mater. 9/2021). Advanced Energy Materials, 2021, 11, 2170036.	10.2	0